Enhancing Hydrogen Adsorption on SnS_2 and $SnSe_2$ Monolayers: Alkali and Alkaline Earth Metal Decoration Under External Electric Fields

(Supplementary Information)

Audomsak Sripothongnack,[a] Watcharin Teeranattapong,[a] Supparat Charoenphon,[a] Adisak Boonchun,[a] Thanayut Kaewmayara,[b] and Pakpoom Reunchan[a*]

[a]*Department of Physics, Faculty of Science, Kasetsart University, Bangkok 10900, Thailand*

[b]*Department of Physics, Faculty of Science, Khon Kaen University, Mueang Khon Kaen, Khon Kaen 40002, Thailand*

*Email: pakpoom.r@ku.ac.th

A. Phonon dispersion of SnS_2 and $SnSe_2$ monolayers

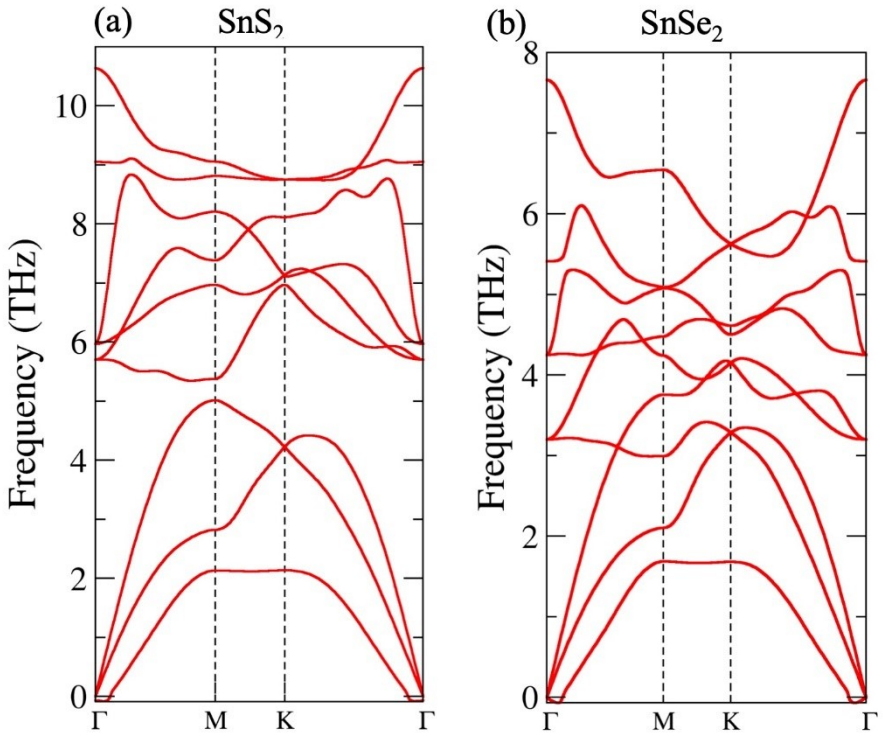

Fig. S1 Phonon dispersion spectra of (a) SnS_2 and (b) $SnSe_2$ monolayers. Both systems exhibit no significant imaginary frequencies across the Brillouin zone, confirming their dynamical stability. The minor negative frequency observed near the Γ point is attributed to numerical artifacts that can arise from factors such as the finite supercell size, the choice of pseudopotentials, or the convergence thresholds. Such minor deviations are common in first-principles phonon calculations and do not affect the conclusion that SnS_2 and $SnSe_2$ monolayers are dynamically stable. Similar behavior has been reported for $SnSe_2$[1] and other 2D materials in the literature.[2]

B. Numerical values of binding energies and cohesive energies

Table S1 Calculated binding energies (in eV) of Li, Na, K, Mg, and Ca atoms on SnS_2 and $SnSe_2$ monolayers at the M and J adsorption sites. The cohesive energy (E_{coh}) of each metal atom is also listed for comparison.

Metal	E_{coh}	SnS_2		$SnSe_2$	
		M-site	J-site	M-site	J-site
Li	-1.669	-2.837	-2.847	-2.947	-2.961
Na	-1.185	-2.360	-2.365	-2.468	-2.434
K	-0.857	-2.577	-2.568	-2.676	-2.673
Mg	-1.692	-2.280	-1.762	-2.564	-2.239
Ca	-1.991	-3.799	-3.332	-3.950	-3.684

Table S2 Calculation of formation energies (in eV) of Li, Na, K, Mg, and Ca on SnS_2 and $SnSe_2$ monolayers at the M and J adsorption sites

Metal	$SnSe_2$		SnS_2	
	M-site	J-site	M-site	J-site
Li	-1.278	-1.292	-0.877	-1.178
Na	-1.284	-1.249	-0.860	-1.181
K	-1.819	-1.815	-1.451	-1.711
Mg	-0.872	-0.546	-0.320	-0.069
Ca	-1.959	-1.694	-1.523	-1.341

C. Atomic structure and charge difference of pristine and metal-decorated $SnSe_2$

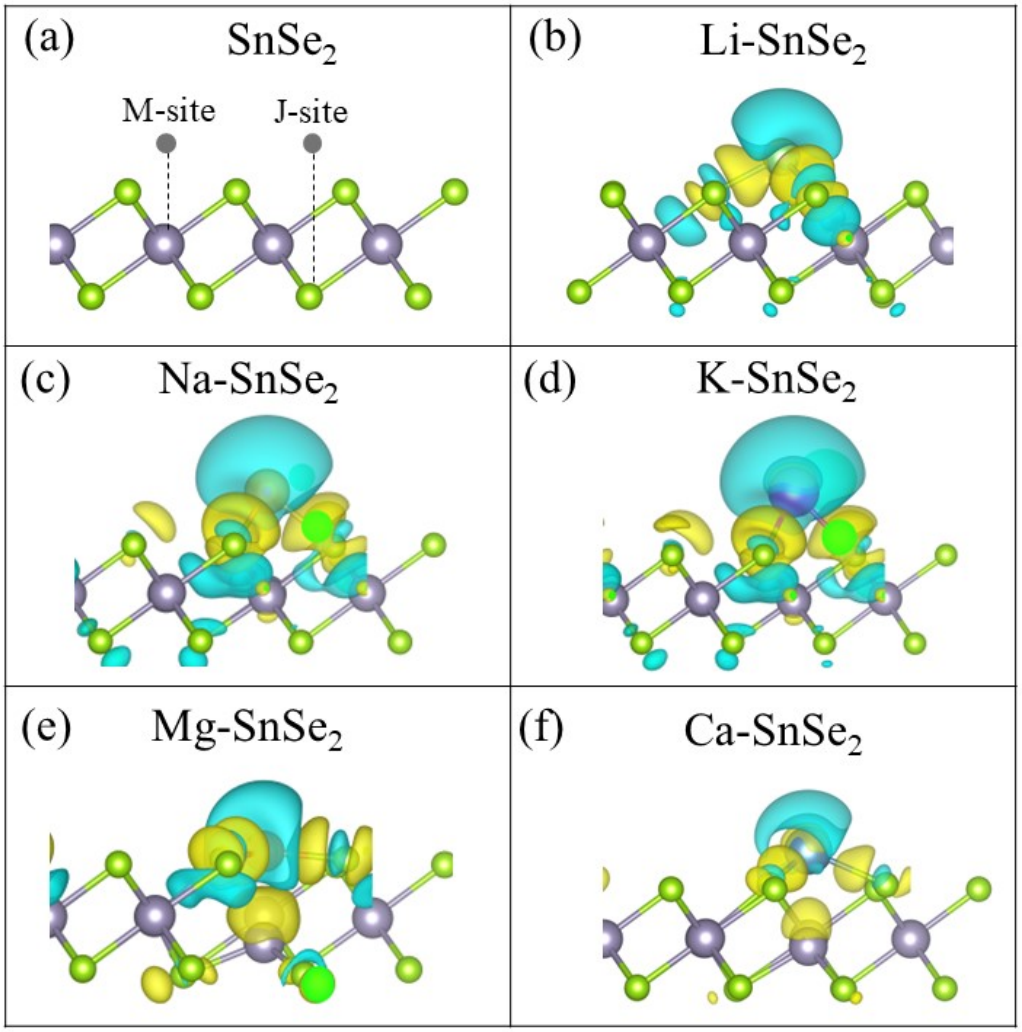

Fig. S2 Optimized atomic structures and charge difference distributions for pristine and metal-decorated SnS_2 monolayers. (a) Pristine $SnSe_2$ monolayer showing the two potential adsorption sites: the M site (above the Sn atom) and the J site (above the lower-layer S atom). Panels (b–f) show the optimized structures of $SnSe_2$ with adsorbed Li, Na, K, Mg, and Ca atoms, respectively, occupying the M site. The overlaid charge difference maps depict regions of charge accumulation (yellow) and charge depletion (blue), illustrating the redistribution of electron density upon metal adsorption.

D. Ab-Initio Molecular Dynamics (AIMD) simulations for single-metal decoration

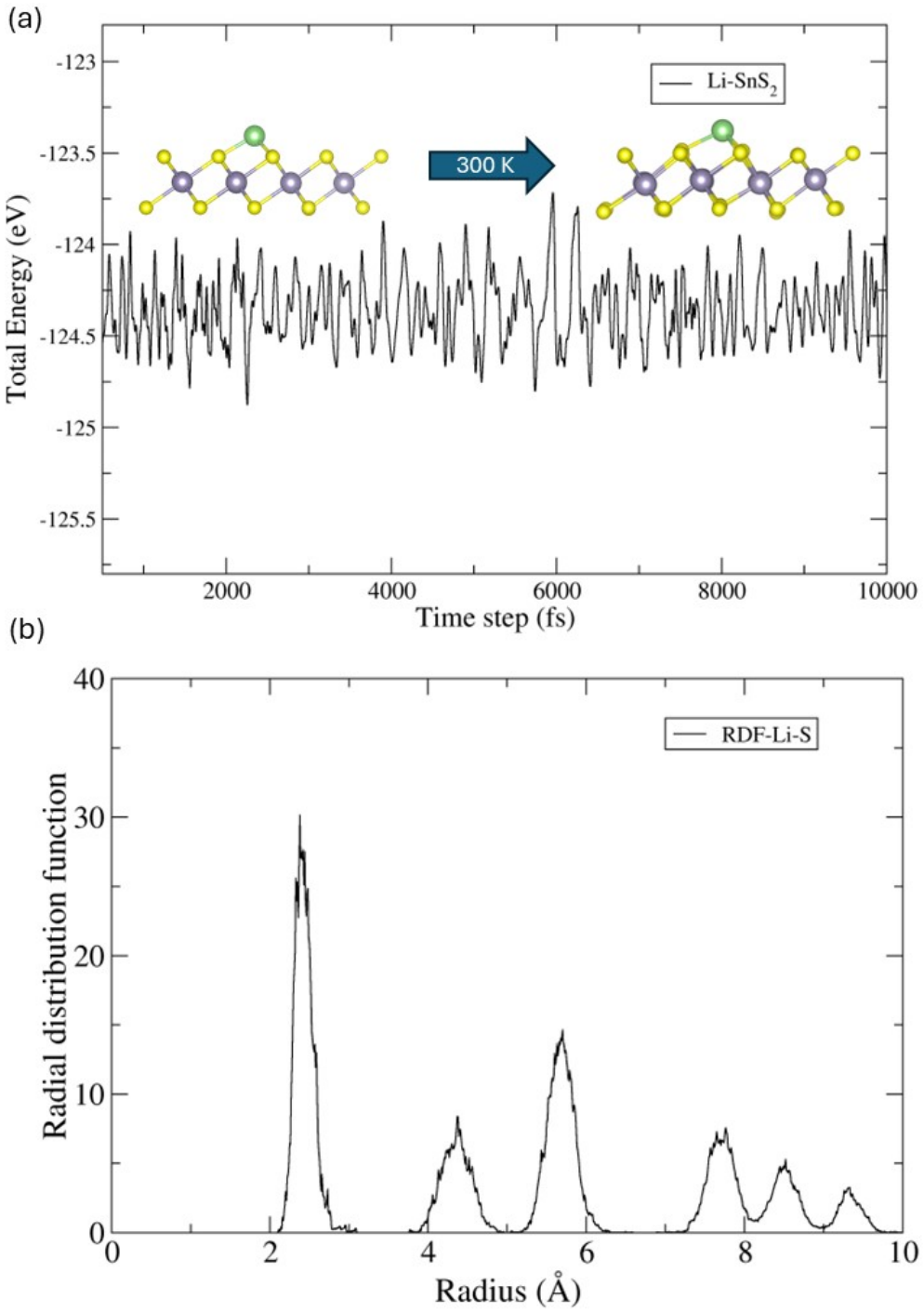

Fig. S3 (a) shows the results of Ab Initio Molecular Dynamics (AIMD) simulations for the Li–SnS_2 system, whereas Figure (b) illustrates the radial distribution function between Li and S atoms.

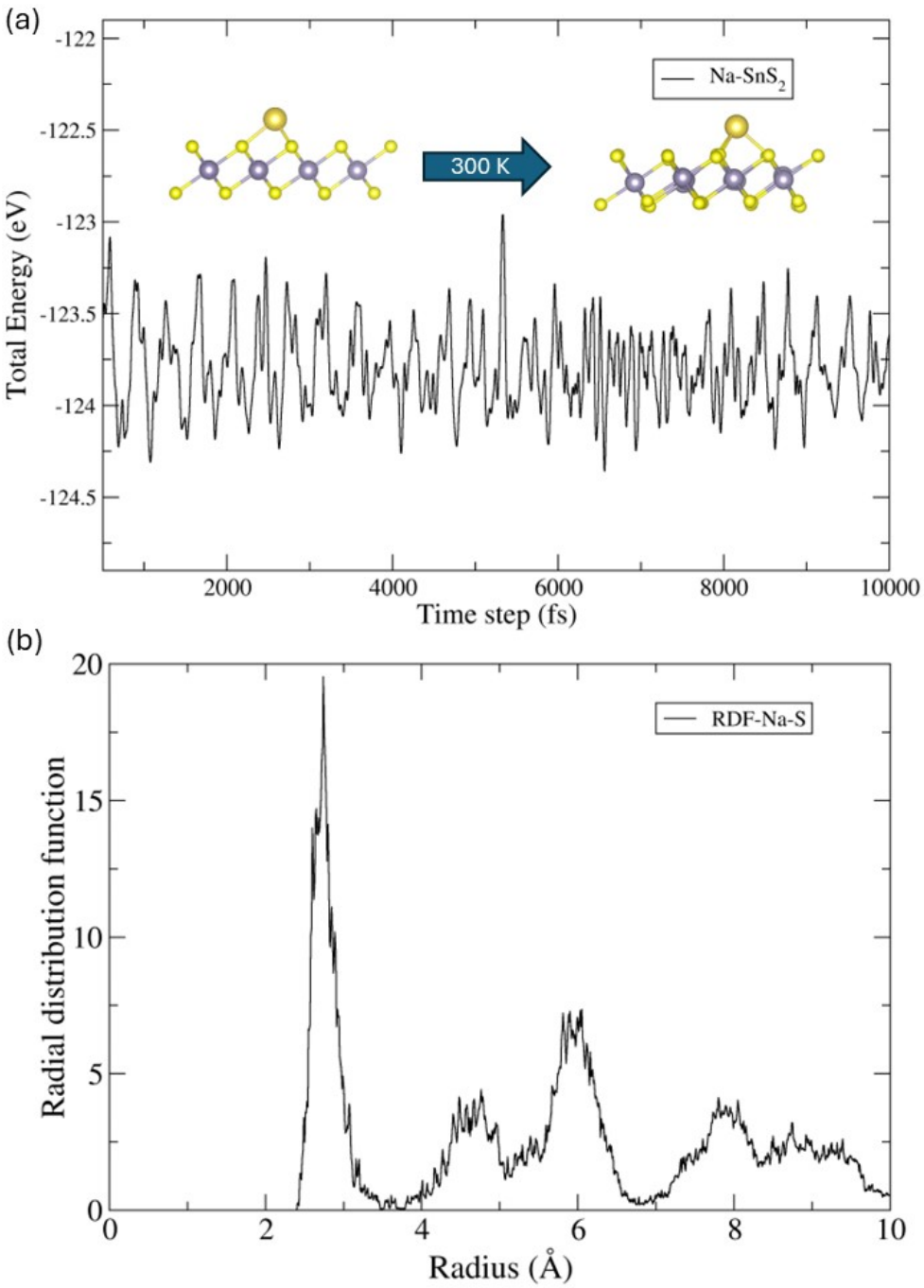

Fig. S4 (a) shows the results of Ab Initio Molecular Dynamics (AIMD) simulations for the Na–SnS_2 system, whereas Figure (b) illustrates the radial distribution function between Na and S atoms.

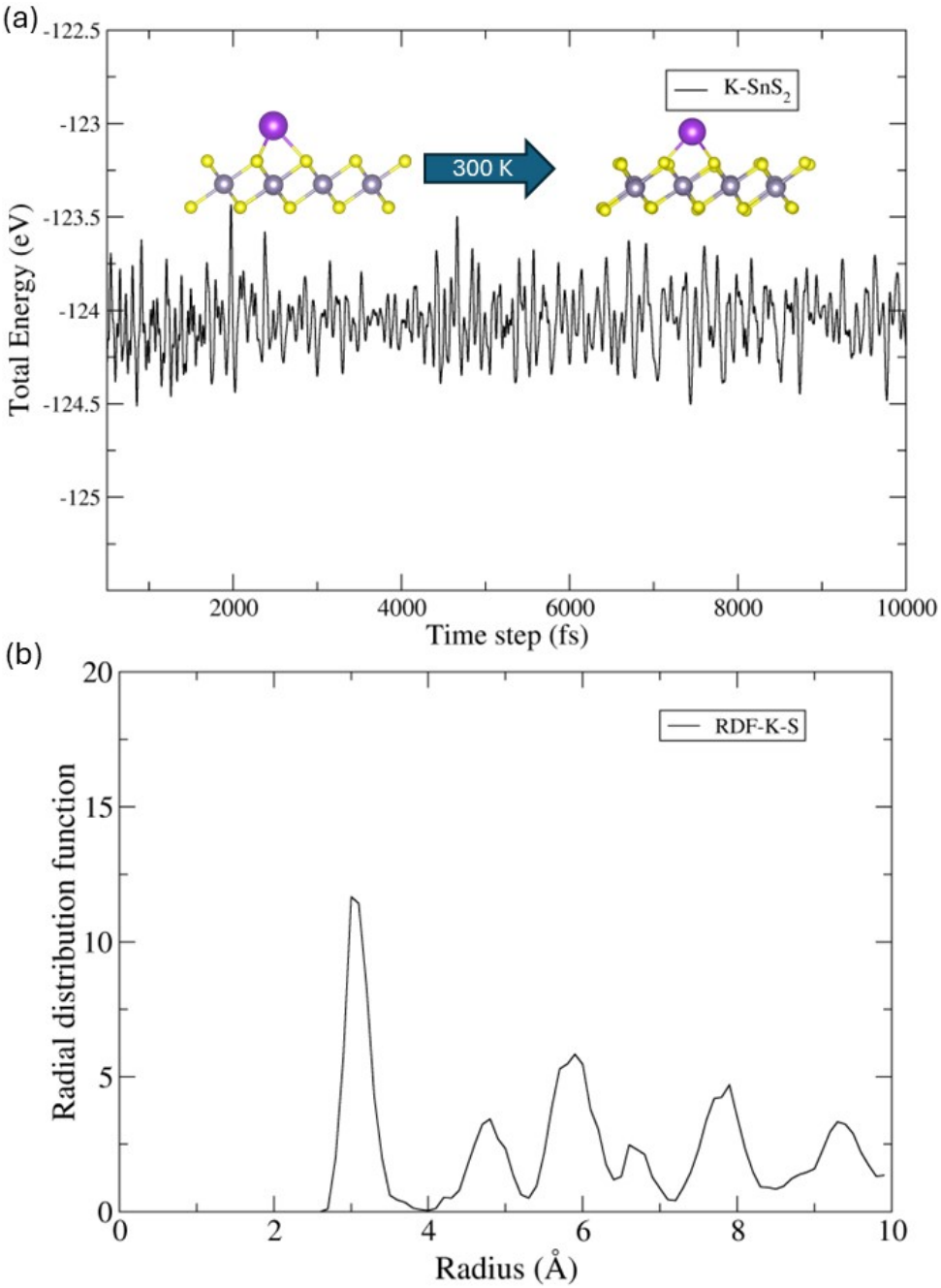

Fig. S5 (a) shows the results of Ab Initio Molecular Dynamics (AIMD) simulations for the K–SnS_2 system, whereas Figure (b) illustrates the radial distribution function between K and S atoms.

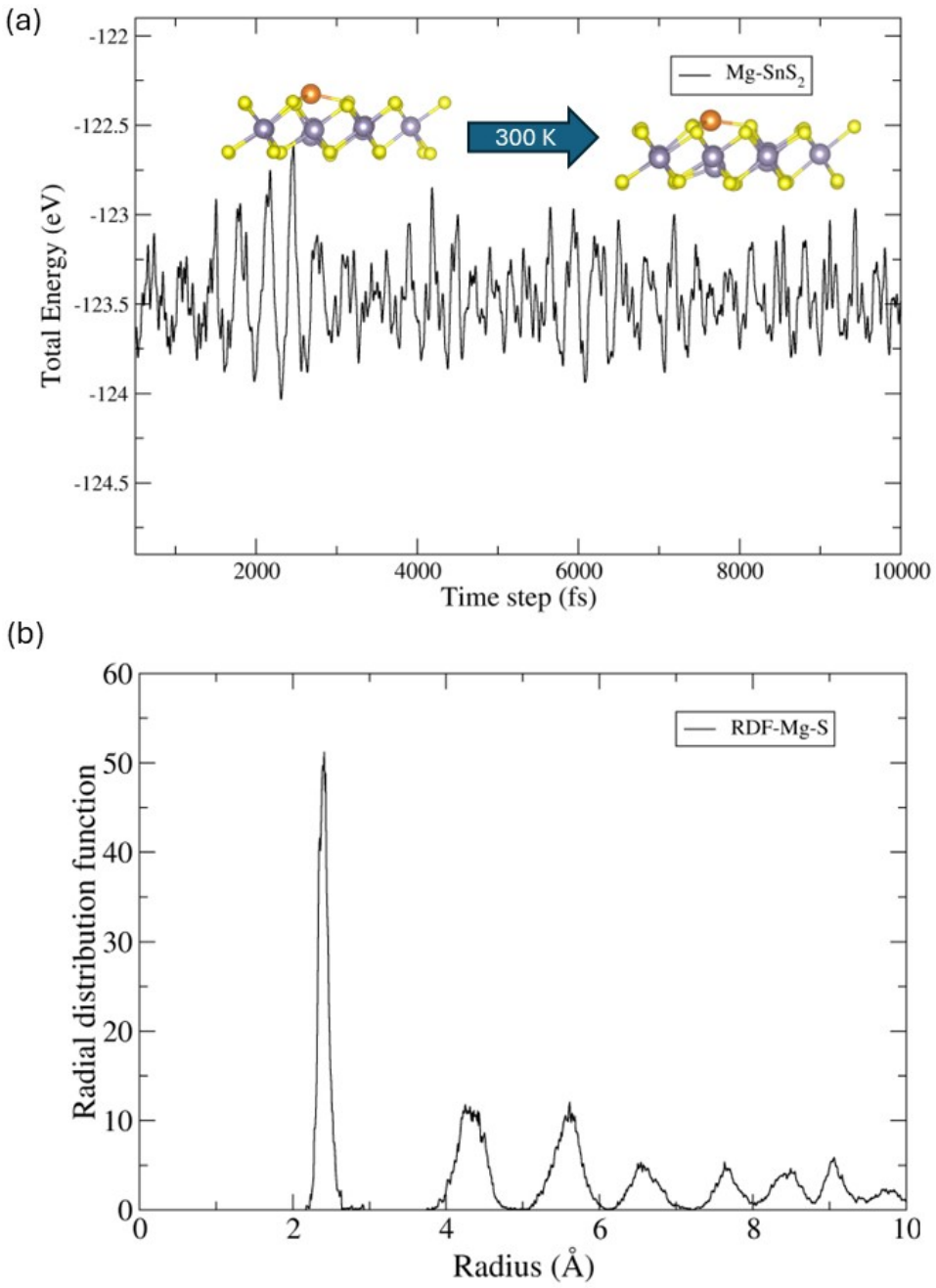

Fig. S6 (a) shows the results of Ab Initio Molecular Dynamics (AIMD) simulations for the Mg–SnS_2 system, whereas Figure (b) illustrates the radial distribution function between Mg and S atoms.

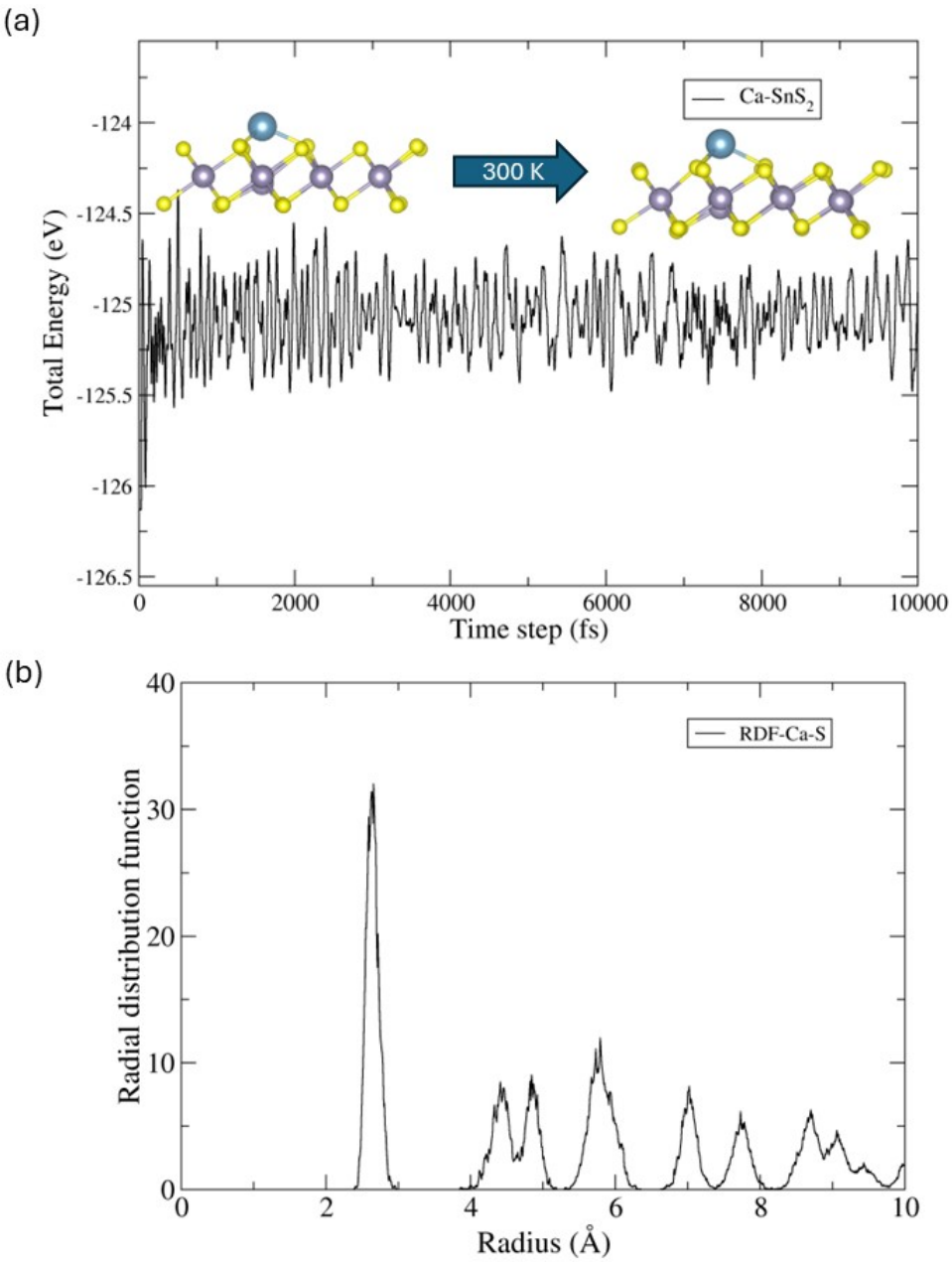

Fig. S7 (a) shows the results of Ab Initio Molecular Dynamics (AIMD) simulations for the Ca–SnS_2 system, whereas Figure (b) illustrates the radial distribution function between Ca and S atoms.

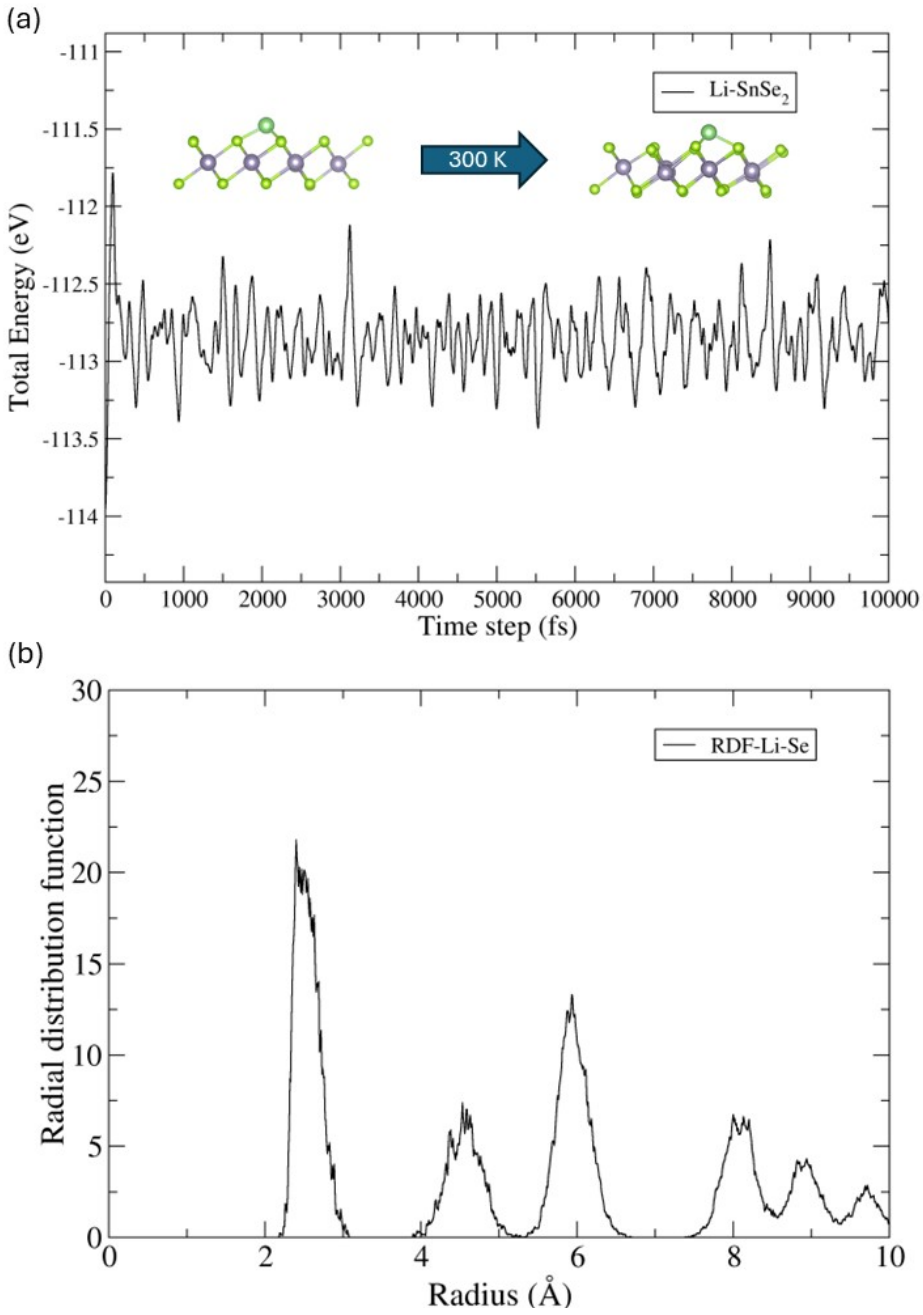

Fig. S8 (a) shows the results of Ab Initio Molecular Dynamics (AIMD) simulations for the Li–$SnSe_2$ system, whereas Figure (b) illustrates the radial distribution function between Li and S atoms.

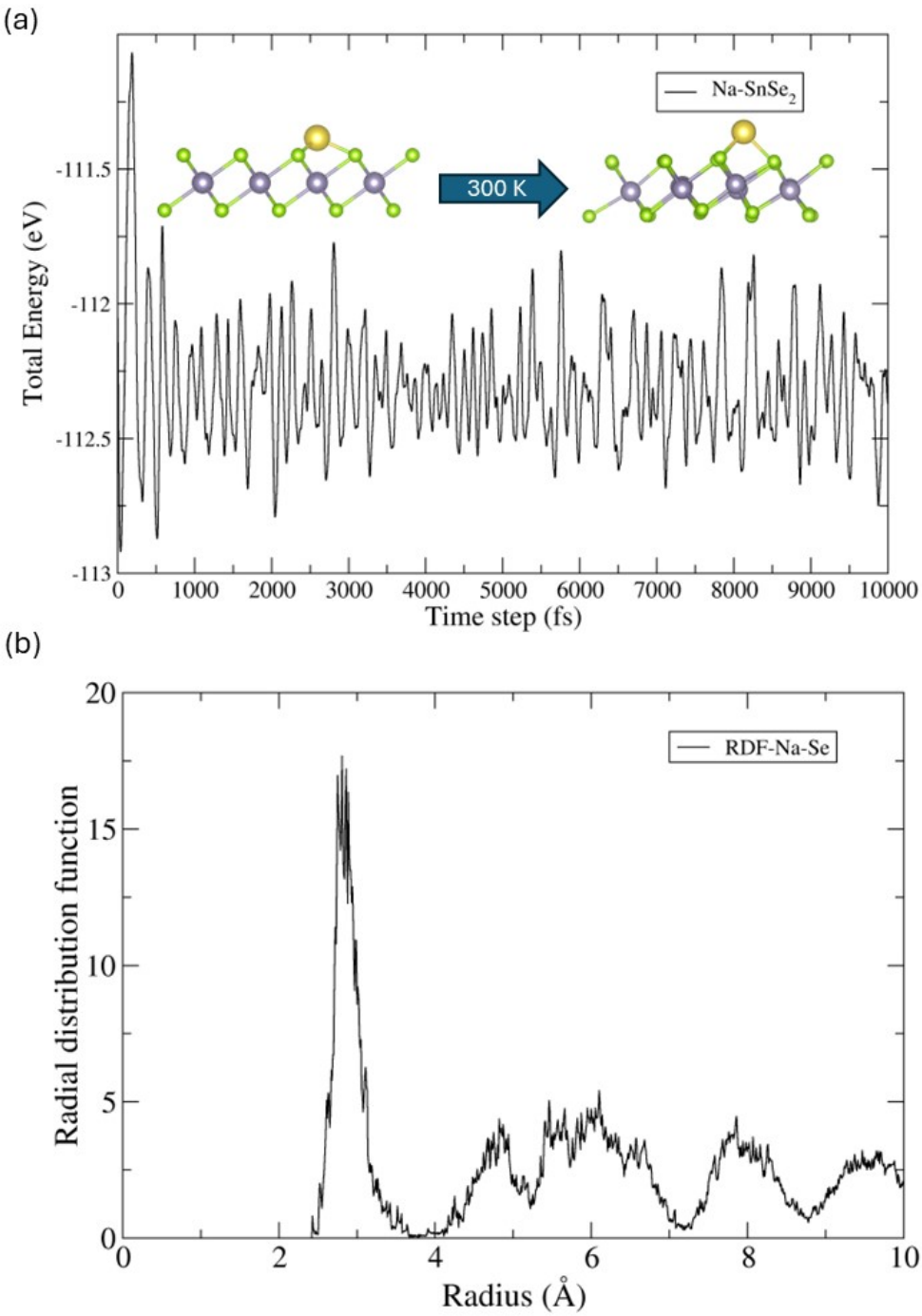

Fig. S9 (a) shows the results of Ab Initio Molecular Dynamics (AIMD) simulations for the Na–$SnSe_2$ system, whereas Figure (b) illustrates the radial distribution function between Na and Se atoms.

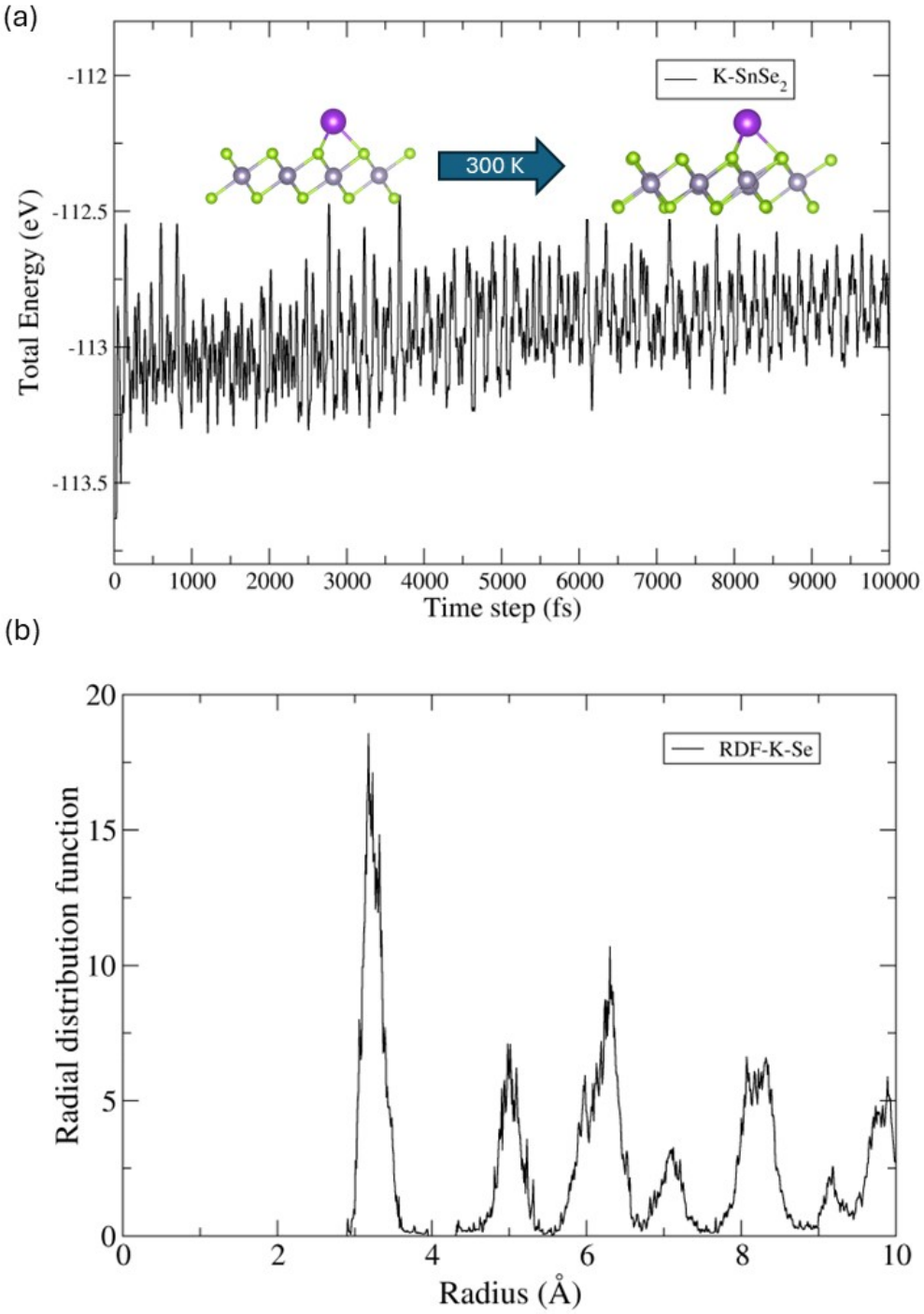

Fig. S10 (a) shows the results of Ab Initio Molecular Dynamics (AIMD) simulations for the K–$SnSe_2$ system, whereas Figure (b) illustrates the radial distribution function between K and Se atoms.

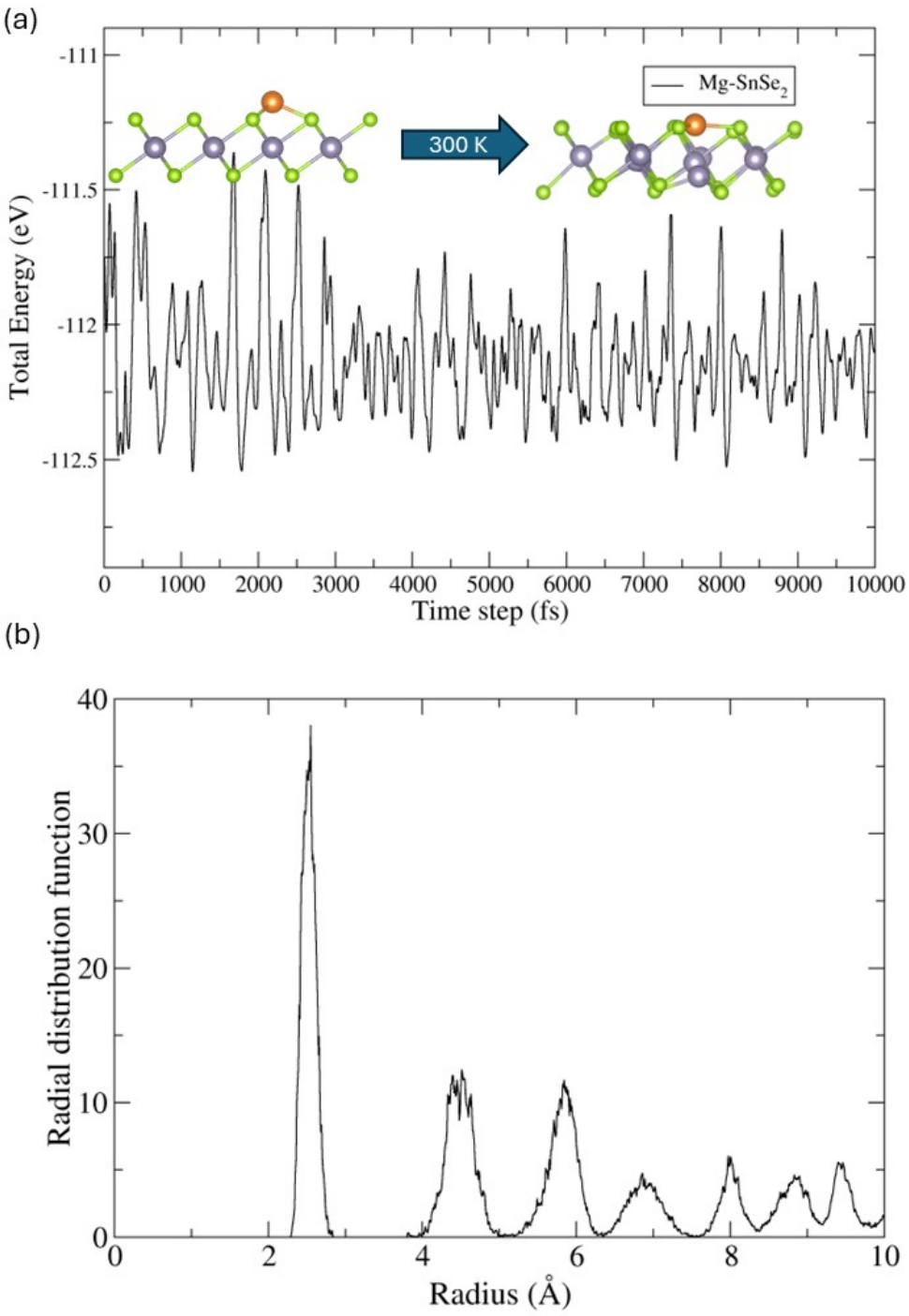

Fig. S11 (a) shows the results of Ab Initio Molecular Dynamics (AIMD) simulations for the Mg–$SnSe_2$ system, whereas Figure (b) illustrates the radial distribution function between Mg and Se atoms.

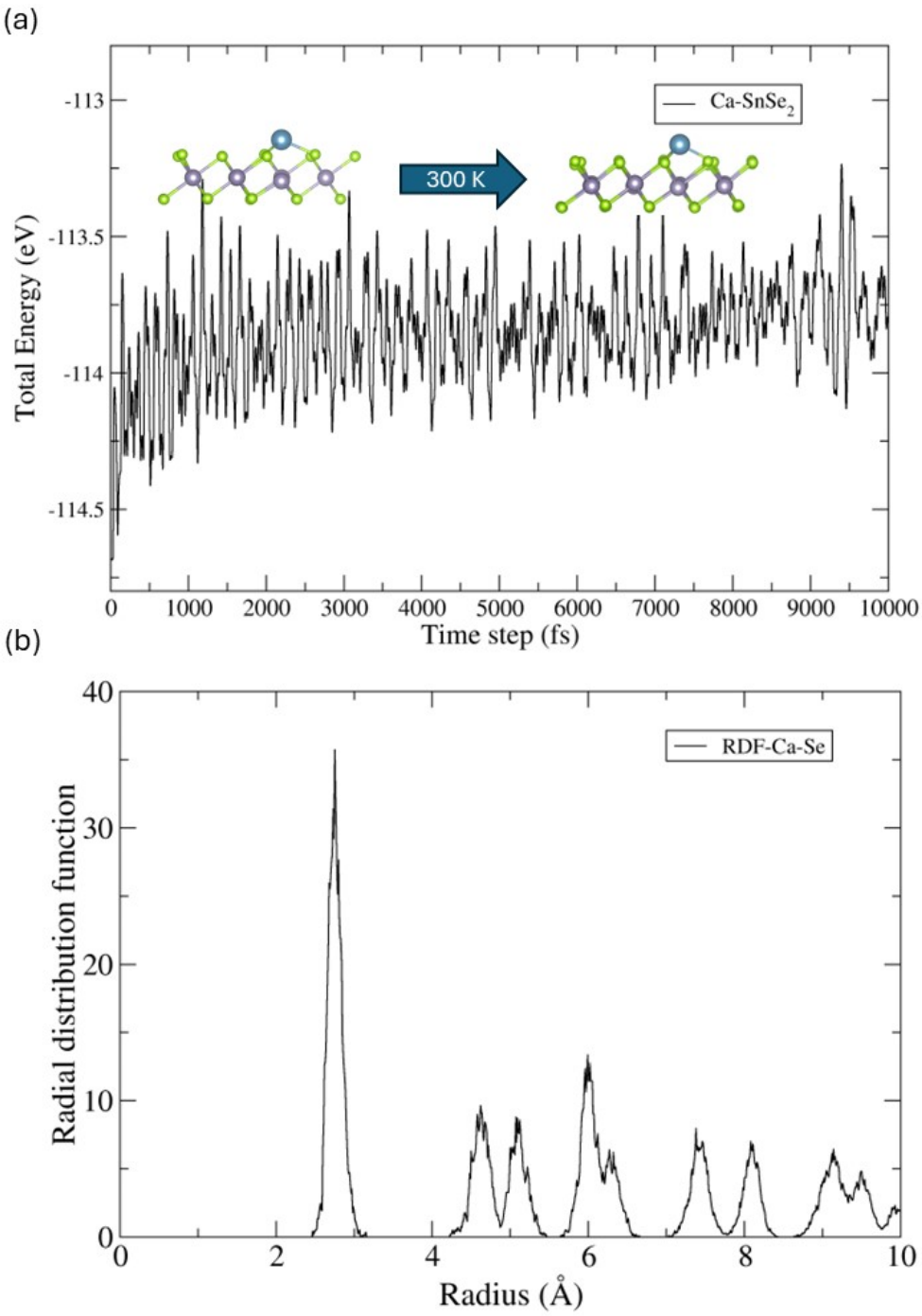

Fig. S12 (a) shows the results of Ab Initio Molecular Dynamics (AIMD) simulations for the Ca–$SnSe_2$ system, whereas Figure (b) illustrates the radial distribution function between Ca and Se atoms.

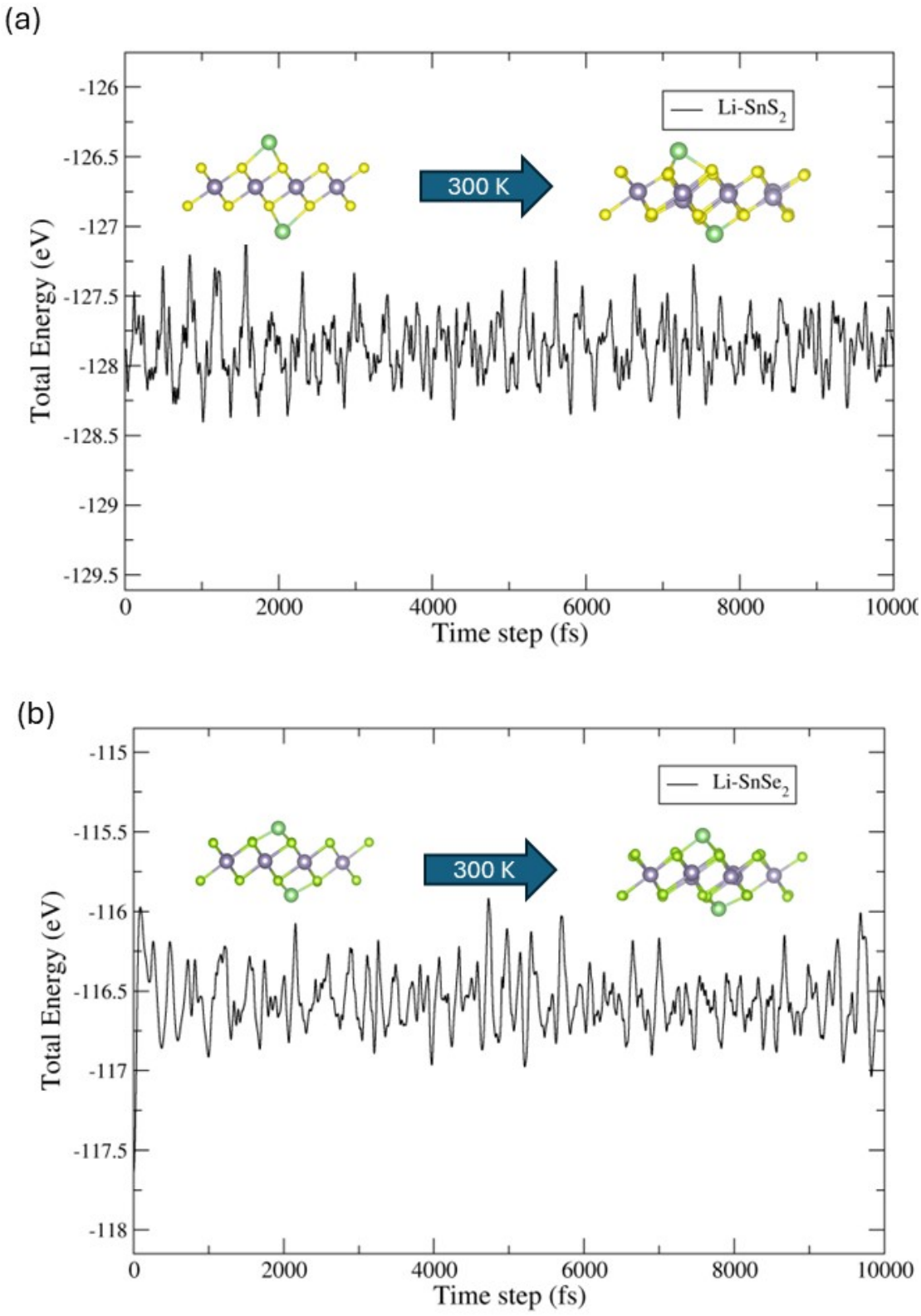

Fig. S13 AIMD simulations for Li–SnS_2 (a) and Li–$SnSe_2$ (b) at 300 K under an external electric field of −0.5 V/Å showing stable energy fluctuation and preserved structural integrity over 10 ps.

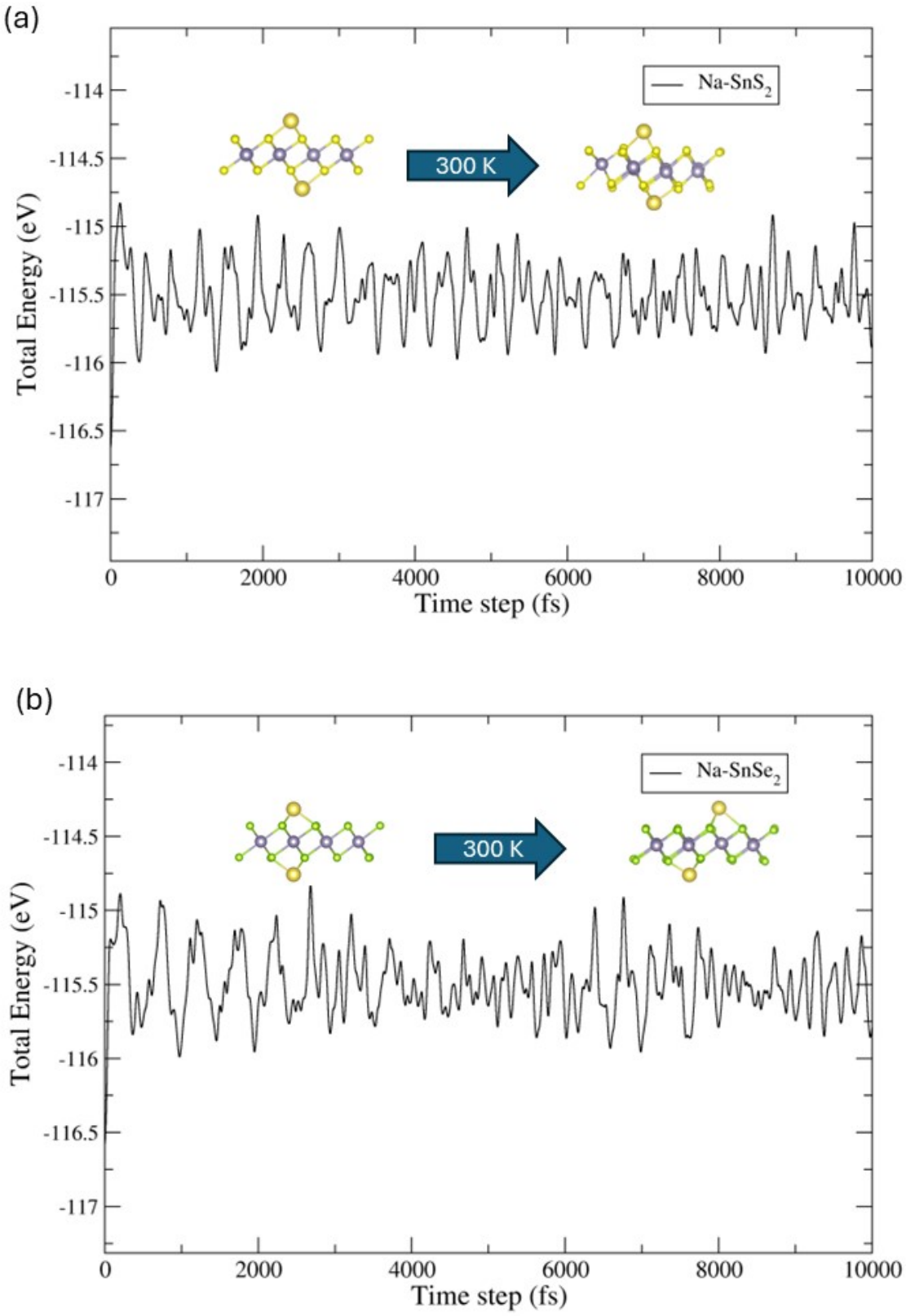

Fig. S14 AIMD simulations for Na–SnS_2 (a) and Na–$SnSe_2$ (b) at 300 K under an external electric field of −0.5 V/Å showing stable energy fluctuation and preserved structural integrity over 10 ps.

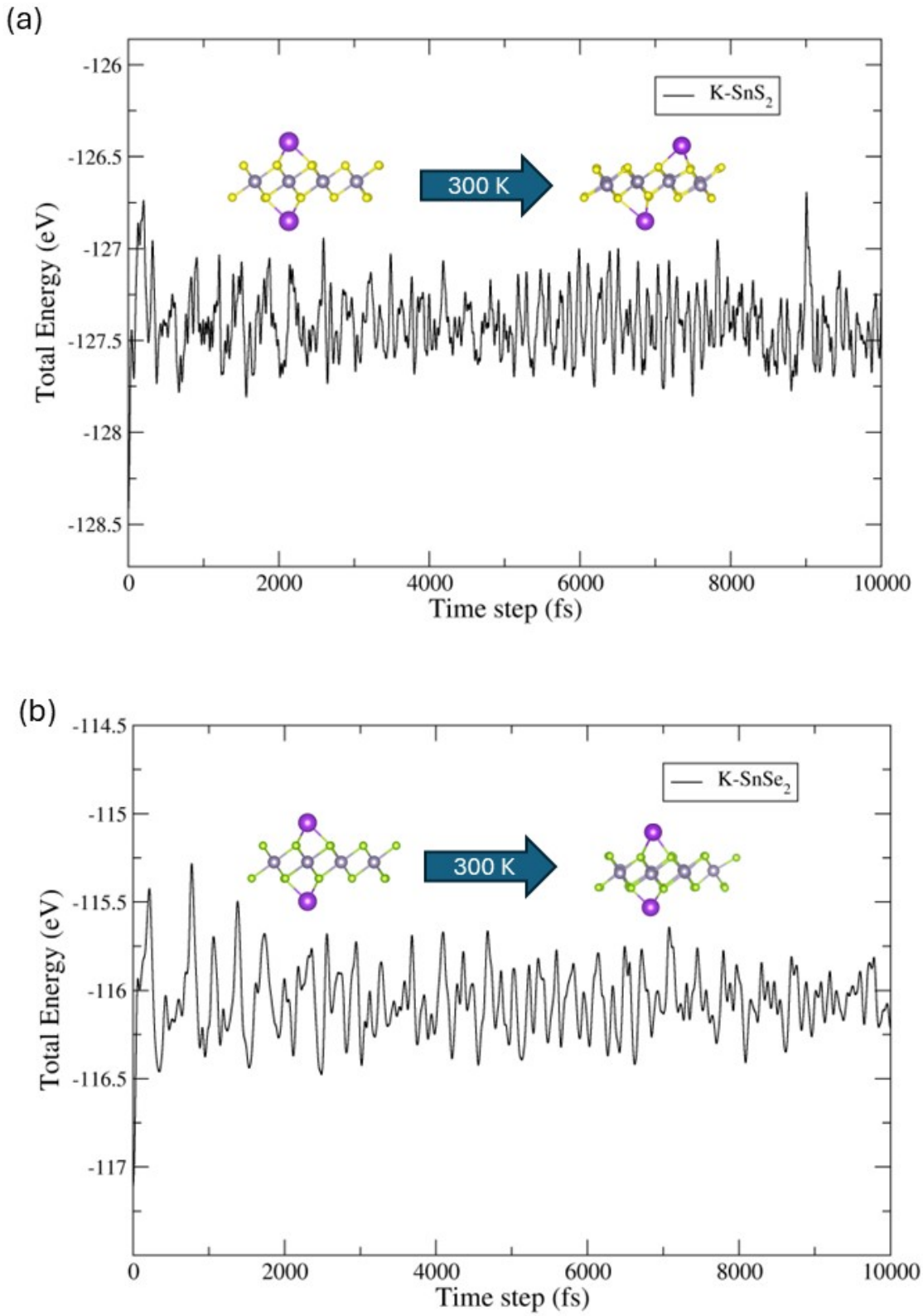

Fig. S15 AIMD simulations for K–SnS_2 (a) and K–$SnSe_2$ (b) at 300 K under an external electric field of −0.5 V/Å showing stable energy fluctuation and preserved structural integrity over 10 ps.

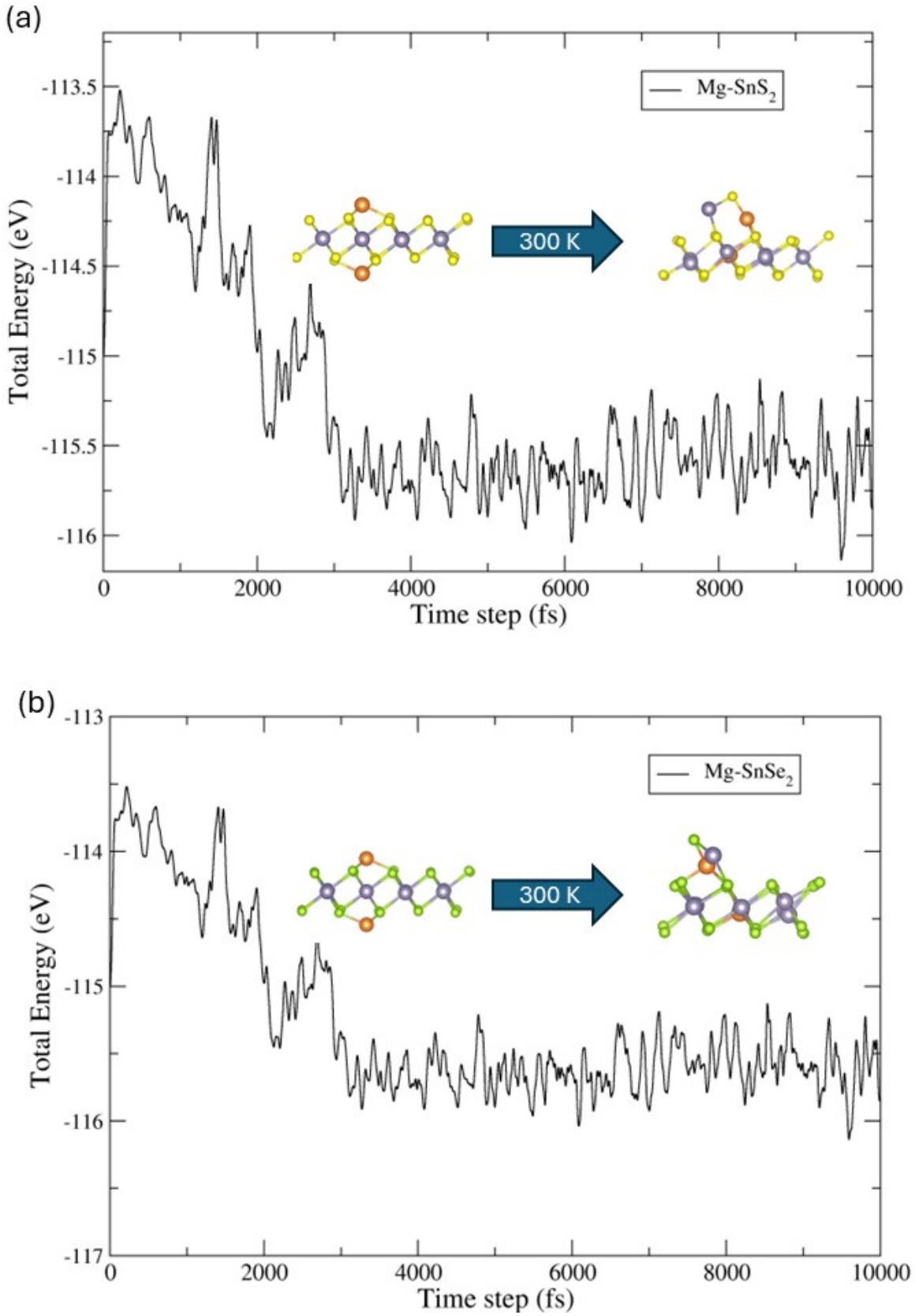

Fig. S16 AIMD simulations for Mg–SnS_2 (a) and Mg–$SnSe_2$ (b) at 300 K under an external electric field of −0.5 V/Å showing unstable energy fluctuation and preserved structural integrity over 10 ps.

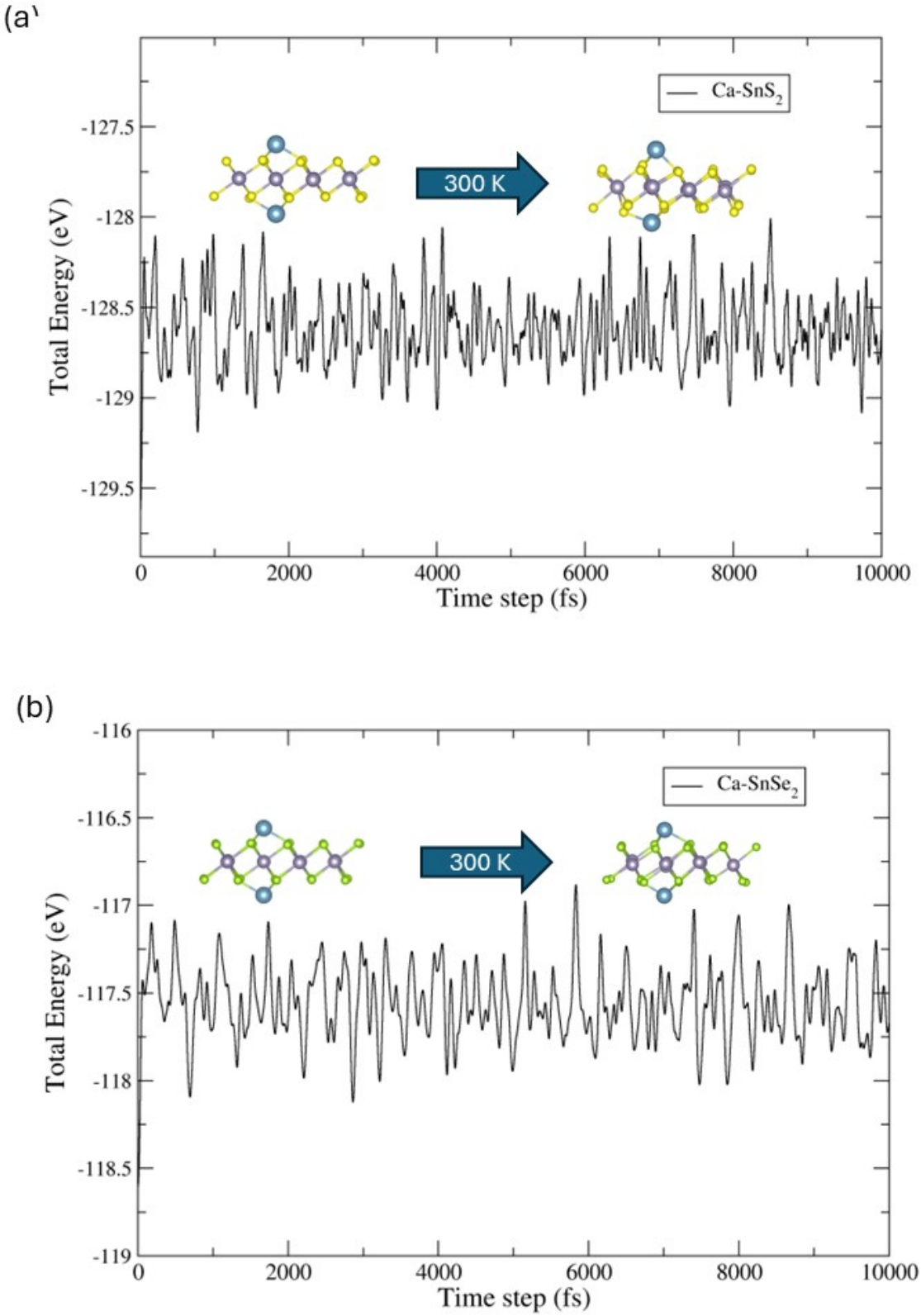

Fig. S17 AIMD simulations for Ca–SnS_2 (a) and Ca–$SnSe_2$ (b) at 300 K under an external electric field of −0.5 V/Å showing stable energy fluctuation and preserved structural integrity over 10 ps.

E. The maximum H_2 coverage configurations for other metal-SnX_2 systems and their Density of states

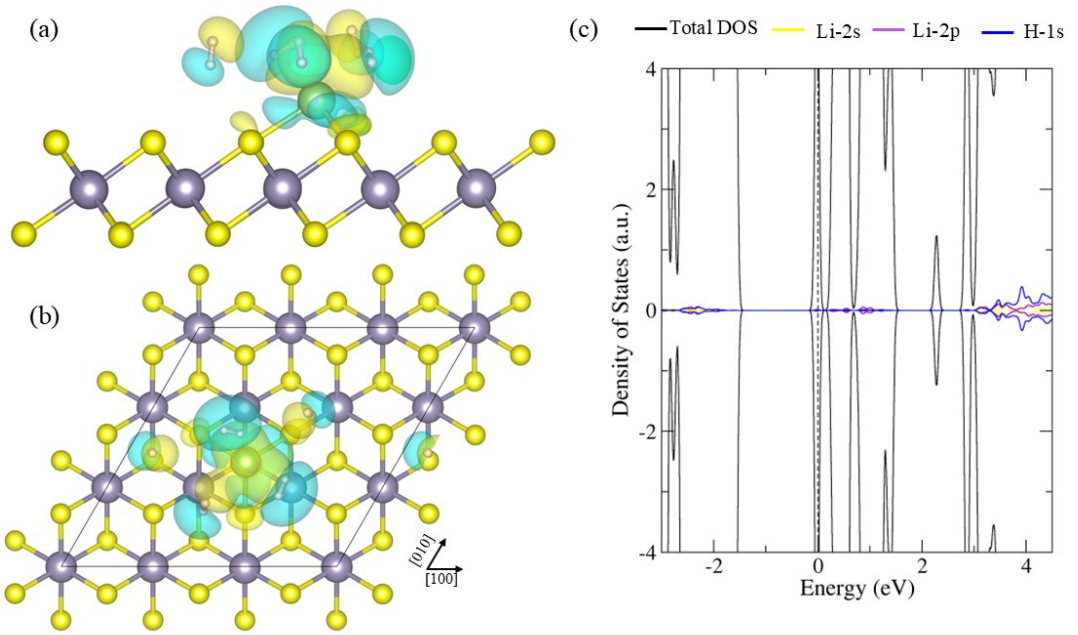

Fig. S18 (a, b) Side and top views of the most stable Li-SnS_2 configuration at maximum H_2 coverage and (c) density of states of the same configuration.

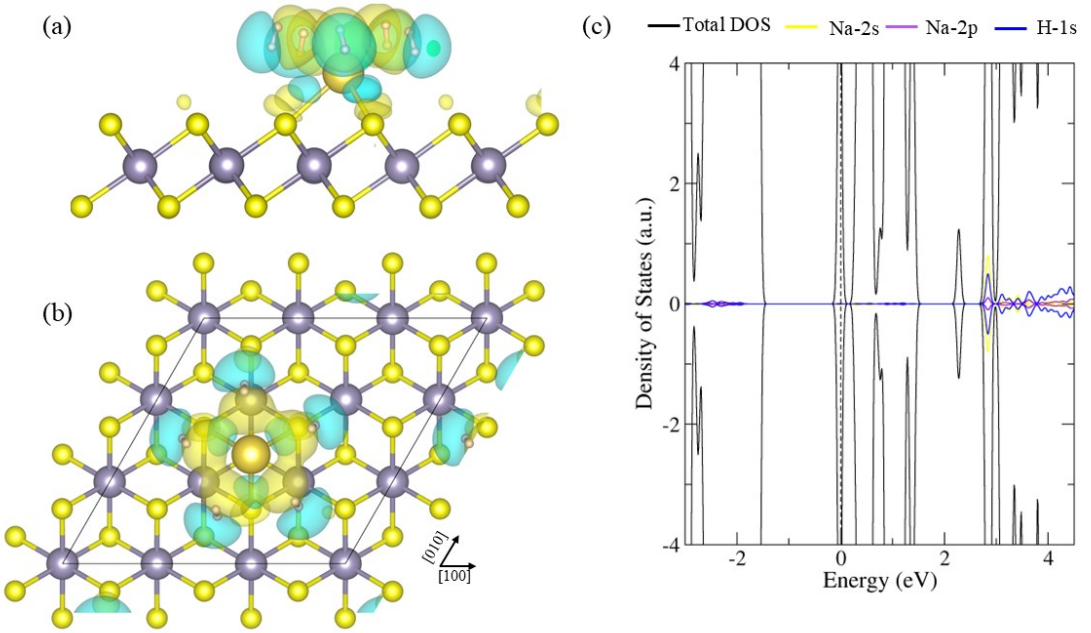

Fig. S19 (a, b) Side and top views of the most stable Na-SnS_2 configuration at maximum H_2 coverage and (c) density of states of the same configuration.

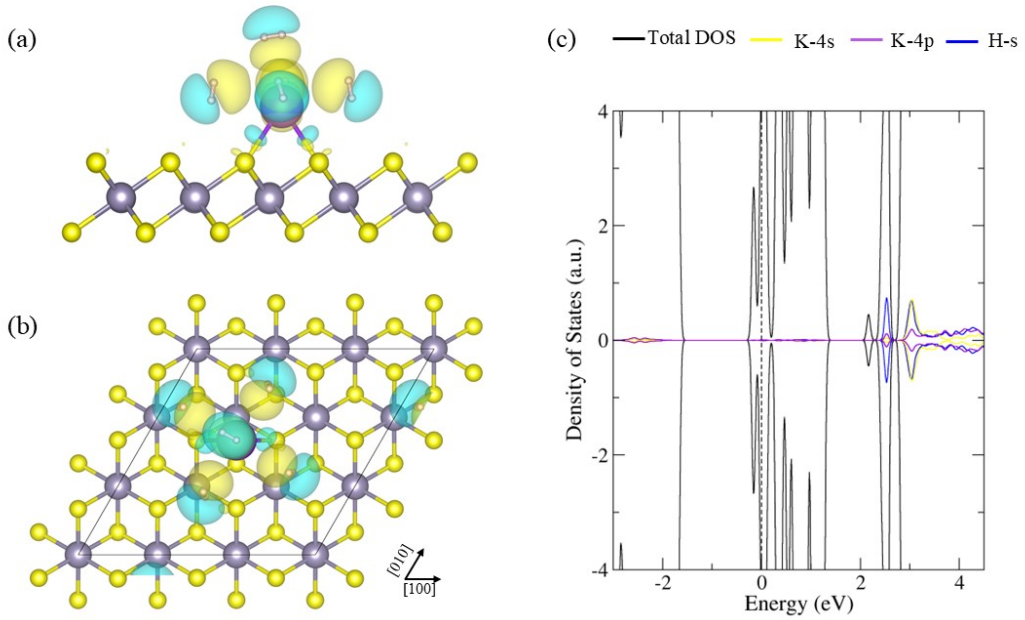

Fig. S20 (a, b) Side and top views of the most stable K-SnS_2 configuration at maximum H_2 coverage and (c) density of states of the same configuration.

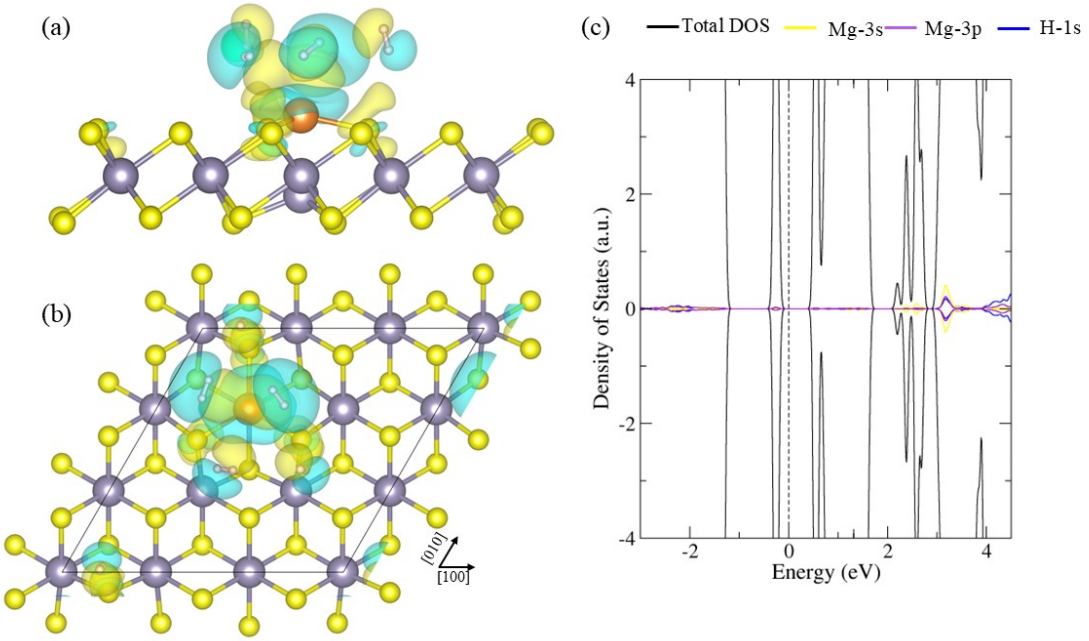

Fig. S21 (a, b) Side and top views of the most stable Mg-SnS_2 configuration at maximum H_2 coverage and (c) density of states of the same configuration.

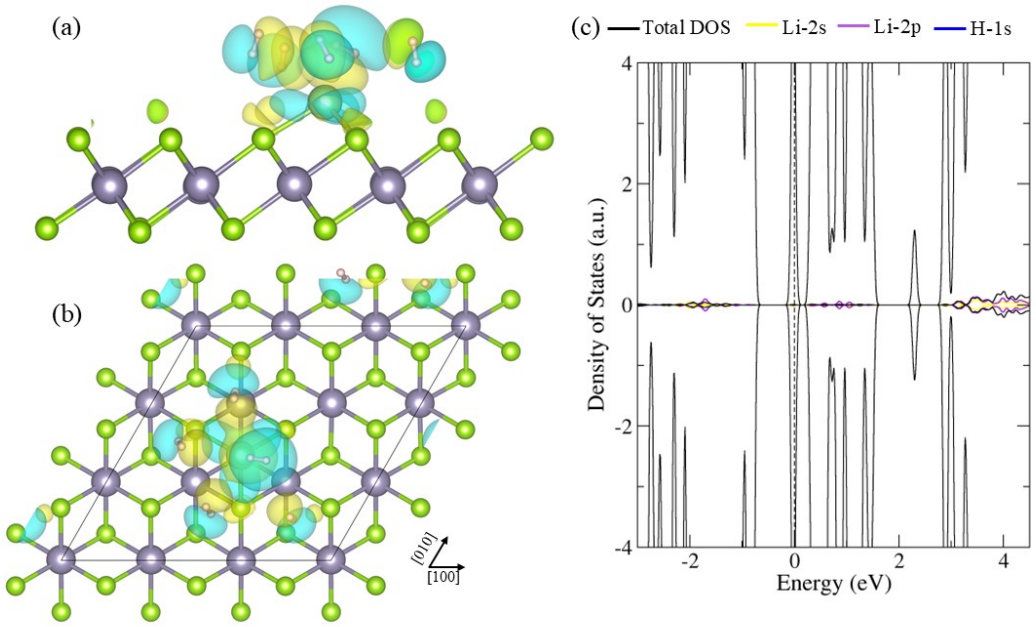

Fig. S22 (a, b) Side and top views of the most stable Li-$SnSe_2$ configuration at maximum H_2 coverage and (c) density of states of the same configuration.

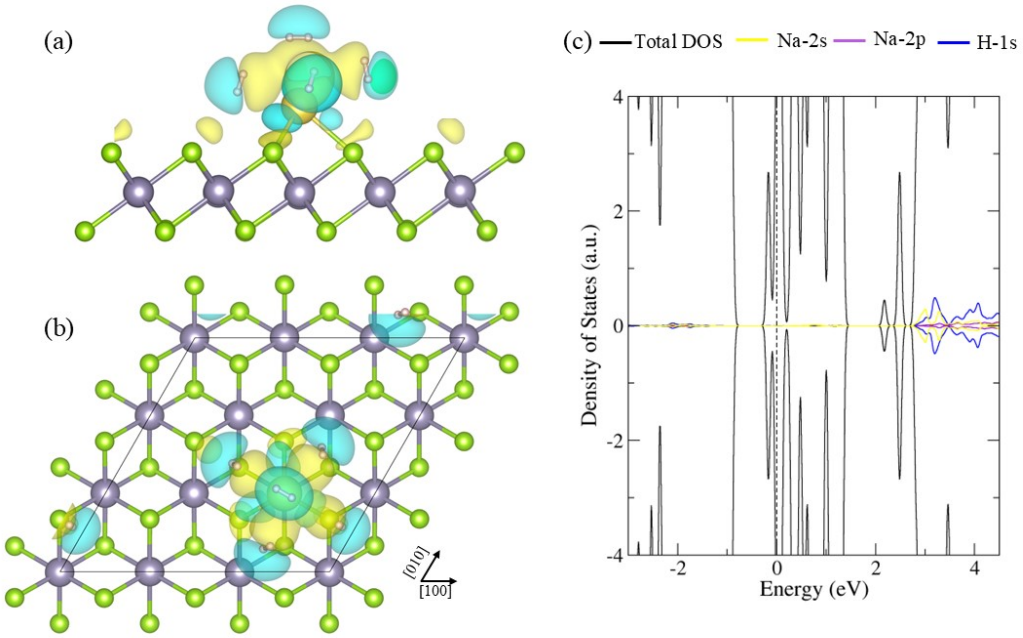

Fig. S23 (a, b) Side and top views of the most stable Na-$SnSe_2$ configuration at maximum H_2 coverage and (c) density of states of the same configuration.

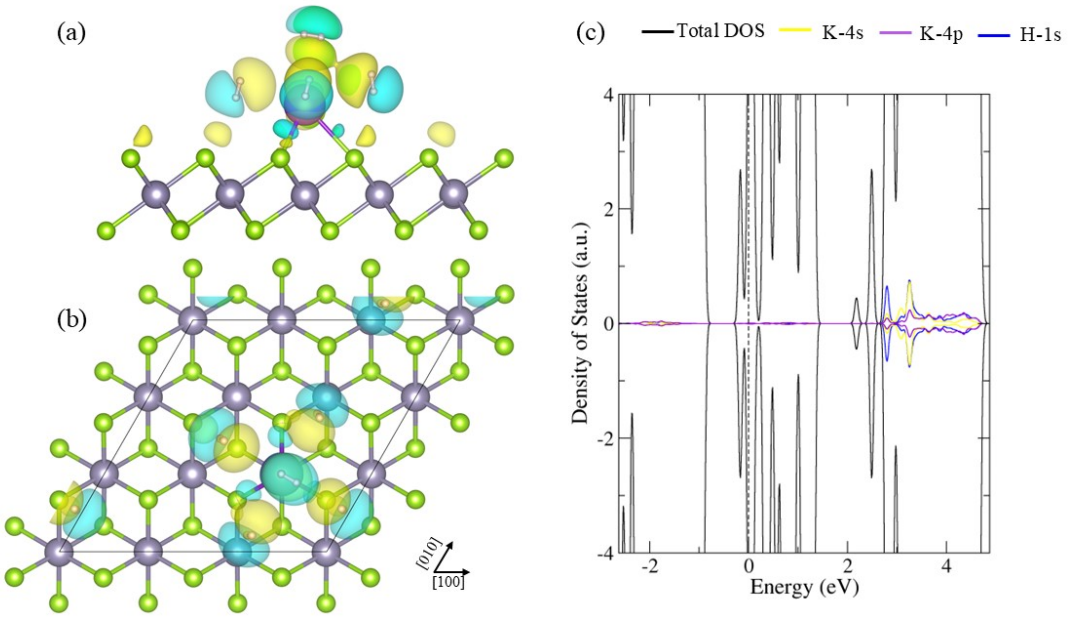

Fig. S24 (a, b) Side and top views of the most stable K-$SnSe_2$ configuration at maximum H_2 coverage and (c) density of states of the same configuration.

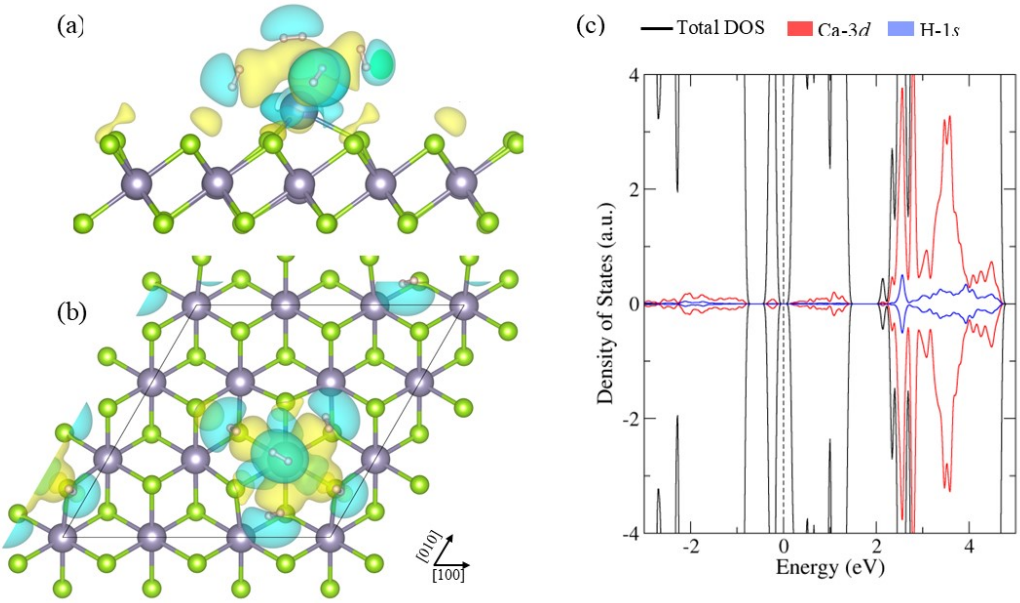

Fig. S25 (a, b) Side and top views of the most stable Ca-$SnSe_2$ configuration at maximum H_2 coverage and (c) density of states of the same configuration.

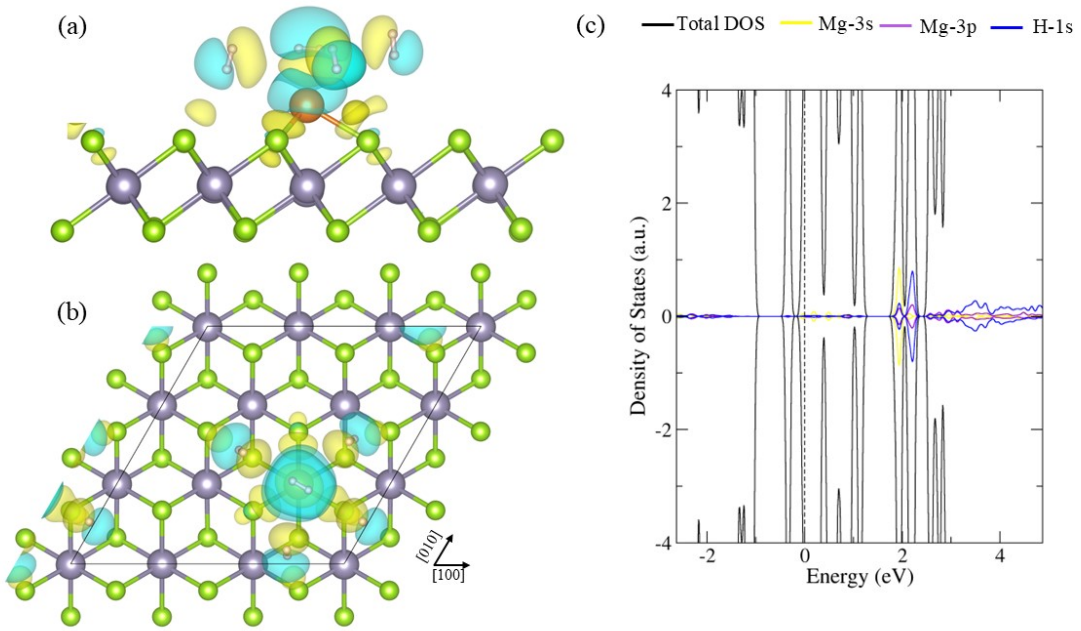

Fig. S26 (a, b) Side and top views of the most stable Mg-$SnSe_2$ configuration at maximum H_2 coverage and (c) density of states of the same configuration.

F. Numerical values of desorption temperatures

Table S3 Desorption temperatures in Kelvin of Ca-decorated SnS_2 and $SnSe_2$ under different pressures.

Number of H_2	SnS_2			$SnSe_2$		
	0.1	1	10	0.1	1	10
1-H_2	166.85	200.64	246.10	149.37	179.68	222.62
2-H_2	171.10	205.29	251.71	169.47	203.50	249.61
3-H_2	171.10	205.29	251.71	166.96	200.76	246.24
4-H_2	159.20	191.50	235.82	156.28	187.98	231.90
5-H_2	141.35	170.02	211.84	139.97	168.37	209.99

References

[1] E. Mohebbi, E. Pavoni, L. Pierantoni, P. Stipa, E. Laudadio, D. Mencarelli, Effect of different pseudopotentials on the phonon frequencies, dielectric constant, and Born effective charge of SnSe and $SnSe_2$ nanostructures: A density functional perturbation theory study, Journal of Physics and Chemistry of Solids, 185 (2024) 111755.
[2] N.F. Martins, J.A.S. Laranjeira, K.A.L. Lima, L.A. Cabral, L.A. Ribeiro, J.R. Sambrano, HOP-graphene: A high-capacity anode for Li/Na-ion batteries unveiled by first-principles calculations, Applied Surface Science, 710 (2025) 163737.